Polymer Bulletin (2022) 79:10595–10613
https://doi.org/10.1007/s00289-021-04066-1

ORIGINAL PAPER

Green synthesis of chitosan-coated magnetic nanoparticles for drug delivery of oxaliplatin and irinotecan against colorectal cancer cells

Nadia Farmanbar[1] · Sharareh Mohseni[1] · Majid Darroudi[2,3]

Received: 2 August 2021 / Revised: 12 December 2021 / Accepted: 27 December 2021 /
Published online: 6 January 2022

Abstract

Recently, the green synthesizing methods of nanoparticles found their place in the center of attention. In this regard. the synthesis of useful nanoparticles such as the magnetic types, as well as the cases of Chia seeds that can form natural mucilage and function as a capping agent, are recognized of great importance. In this work, superparamagnetic (Fe_3O_4) nanoparticles were prepared by using the water extract of chia seeds for the first time, which was then coated with chitosan (CS), Fe_3O_4@CS core–shell, and finally, exerted for the drug delivery of oxaliplatin (OXA), and irinotecan (IRI) that were labeled as Fe_3O_4–OXA@CS core–shell and Fe_3O_4–IRI@CS core–shell, respectively. The nanoparticles were characterized through the means of XRD, FTIR, UV–Vis, TEM, FESEM, DLS, zeta potential, and VSM. The results of XRD analyses confirmed the successful synthesis of superparamagnetic nanoparticles. The observed crystallity, solid-phase, and hydrodynamic sizes were indicative of particle agglomeration in the solid phase, while in comparison to the crystallite sizes and particle diameters were increased up to more than 3-folds. The occurrence of agglomeration was more apparent in the case of Fe_3O_4–OXA@CS core–shell. Moreover, the cytotoxicities of nano-drugs were investigated against CT-26 cancer cells by the application of MTT (3-(4,5-dimethylthiazol-2-yl)-2,5-diphenyltetrazolium bromide) assay. The IC_{50} values of Fe_3O_4@CS core–shell, Fe_3O_4–OXA@CS core–shell, and Fe_3O_4–IRI@CS core–shell were reported to be 246.6, 79.6, and 61.1 ppm, respectively. The cytotoxicities of drug-loaded nanoparticles were exceedingly increased when being compared to the case of Fe_3O_4@CS core–shell.

Keywords Magnetic nanoparticles · Drug delivery · Colorectal cancer · Core–shell · Biopolymer

✉ Sharareh Mohseni
Sh.mohseni@iauq.ac.ir

✉ Majid Darroudi
darroudim@mums.ac.ir; majiddarroudi@gmail.com

Extended author information available on the last page of the article

Introduction

In past years, hybrid nanomaterials received the attention of many for their applicability in bioapplications, including nano-enabled bioseparation, diagnostics, and drug delivery [1–3]. Among the varying available drug delivery systems (DDSs), the great importance of targeted platforms is undeniably evident due to the higher capacity for improving the efficiency of treatments while minimizing the side effects as well [4–7]. Nanomaterials based on superparamagnetic iron-oxide nanocomposites (SPIONs) can be well-tailored for specific purposes such as cancer therapy. In this regard, the superparamagnetism and facile surface-modification of SPIONs is at the center of attention. At present, the most eminent bioapplications of SPIONs include the development of bioseparation methods, protein and enzyme scaffolds, heterogeneous immunoassay systems, DDSs, and medical imaging. The SPIONs can be externally directed towards the cancer tissues and also, be used to dissipate heat (Hyperthermia) in an external alternating magnetic field [8–16]. Currently, the dose-limiting toxicities of chemo drugs stand as a challenge in clinical applications due to the adverse effects of most chemotherapeutics in physiological conditions. For example, the dose-limiting side effects of oxaliplatin (OXA) and irinotecan (IRI) are known as cumulative neurotoxicities and respiratory failure, respectively [17–19]. One of the circumventing approaches for this matter is the performance of chemo drugs targeted delivery with high toxicities by the utilization of nanocarriers [20, 21]. The magnetic nanoparticles (MNPs) are physiologically stable, biodegradable, and safe [22]. Interactive functionalities on the surface of MNPs can lead to combinatorial advantages such as better biocompatibility, stability, and drug loading capacity [23–29]. Surface decoration with biopolymers provides new surface functionalities that result in binding to active agents and decreasing the inducement of agglomeration/aggregation [30–32]. Although there are coatings that shelter the core and weaken magnetic guidance, yet the commercialized SPIONs (size ~ 30 nm) offer specific surface functionalities designed for particular goals [33]. The MNPs meant for OXA delivery, which is functionalized with pectin, were observed to be capable of performing sustained drug release, effective delivery of active agents, and superb cytotoxicity against MIA-PaCa-2 pancreas cancer cells [34]. Similarly, a combination of radiotherapy and chemotherapy was reported to eradicate lung cancer cells through external magnetic fields for the localization of nanoparticles [35, 36]. Drug efficacy can be also increased by executing Gemcitabine loading onto the surface of chitosan MNPs. The occurrence of a hydrogen bond or electrostatic interactions can stand as the explanation of polar agents loading such as ciprofloxacin onto the surface of chitosan-modified nanomagnets [37]. Furthermore, IRI-loaded nano-complexes of SPIONs and chitosan proved to be a promising candidate for the future treatment of HCT-116 cells throughout in vitro and in vivo cases [38, 39]. As another interesting example, decorated NMPs with cyclodextrins and chitosan can form a hydrophobic interior and hydrophilic exterior while being able to act as efficient water-insoluble agents [40, 41]. In addition, the induced cyclodextrins degradation in colons

can be exerted as a trigger for performing targeted delivery [42]. On the other side regarding DDSs, the interaction of Chitosan, as a polysaccharide with active amines and hydroxyls, with glycoconjugates results in creating an opening for the active agents to pass through the epithelial cells [43, 44]. Thus, it can be indicated that the coating of NMPs with chitosan or the formation of hybrid nanomaterials with MNPs and chitosan can be very beneficial for drug delivery purposes [45]. Synthetic procedures are another aspect in this field that requires specific attention [46]. The synthesis of smaller-sized MNPs with a special morphology is quite challenging. Alternative green methods, such as the usage of plant extracts, provide new sources of capping agents for developing remarkable synthetic procedures, which would give rise to new morphologies and smaller particles. The chia (Salvia hispanica) is originated from the Lamiaceae family and coated with glucose, xylose, and glucuronic acid. It is capable of forming a gel/mucilaginous substance in aqueous media, which can be used as a capping agent for the synthesis of metallic/metal oxide nanoparticles [47–49]. In this study, we introduced a new nanocomposite of MNPs and chitosan and examined its ability in performing the drug delivery of OXA and IRI. The MNPs were synthesized through a co-precipitation method by the usage of chia seed mucilage as a capping agent in water. To the best of our knowledge, this is the first experiment that involves the exertion of chia seed mucilage for synthesizing SPIONs, which could be of great importance from size and morphology standpoints. Recently, chia seed mucilage was used to perform a synthesis that resulted in achieving 7 nm-sized silver nanoparticles with aspherical morphology and, therefore, it seems to be worthy to try the synthesis of other nanoparticles by the application of this mucilage [50]. Herein, the prepared MNPs were fully characterized and their physicochemical properties were analyzed and discussed. Although the main focus of this synthesis was to confirm and investigate the occurrence of changes in structure, magnetism, size, and morphology, however, we also studied the application of prepared MNPs in the drug delivery of OXA and IRI and assessed the cytotoxic effects of prepared nanosystems in annihilating CT-26 colon cancer cells. The effects of loaded nanoparticles on the cell proliferation of cancer cells were determined by the means of MTT (3-(4,5-dimethylthiazol-2-yl)-2,5-diphenyltetrazolium bromide) assay while performing a comparison between the results of IC_{50} cases as well.

Materials and methods

All of the exerted chemicals contained high purity and were procured from Merck Co of Germany. The utilized plant species in this study were natural chia seeds obtained from Iran and Low molecular weight chitosan (Brookfield viscosity 20.000 cps) was purchased of from Merck Co. Synthetic materials were characterized by the employment of UV–Vis spectrophotometry (UV–Vis, Unicode 2100, USA), Fourier transforms infrared spectroscopy (FT-IR, Brucker Tensor 27, USA), powder X-ray diffraction (XRD, Panalytical Company X'pert PRO MPD, Denver, USA), dynamic light scattering (DLS), zeta potential analyzer (Zetasizer Nano ZS,

Malvern, England), transmission electron microscopy (TEM, Metropolitan-Vickers, H9500, England), and field emission scanning electron microscopy (FESEM, HITACHI S4160, Germany).

Chia seeds water extract

Initially, 1.0 g of Chia seeds were weighed and washed several times with distilled water. Then, 50 mL of distilled water (DW) was added to have the solution heated until reaching 60 °C, which was placed under constant stirring for 2 h. Thereafter, the extract was separated and stored in the refrigerator for the upcoming experiments [51].

Synthesis of SPIONs

On this section, 0.18 g of $FeCl_2.4H_2O$ and 0.50 g of $FeCl_3.6H_2O$ (Fe^{2+}: Fe^{3+} ratio = 1:2) were dissolved in 100 mL of DW at room temperature. Then, 30 mL of chia seed extract was added and the mixture was stirred within a nitrogen atmosphere at 45 °C for 20 min. The color was observed to be altered and turned from orange to dark green. After 10 min, NaOH solution (1.0 M) was appended to the mixture until reaching a pH > 9. As the next step, the black precipitate was separated by an external magnet and washed several times with DW. The obtained product was dried at 40 °C for 2 h and used without further purification.

The biosynthesis mechanism of nanoparticles by the usage of plant extract is demonstrated in Fig. 1. The green chemistry method was used to reduce or eliminate

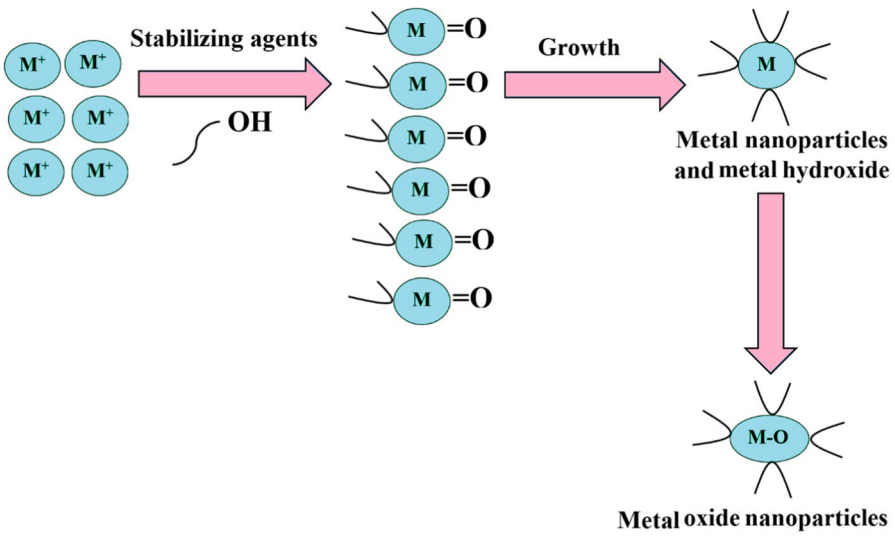

Fig. 1 The biosynthesis mechanism of nanoparticles

hazardous substances in the synthesis process. The chia seed extract has been proposed before as an appropriate material in green synthesis because of its safe nature and ability to act as a reducing agent in nanoparticles synthesis. As an example, Sabouri et al. [52] took benefits from *Salvia hispanica L. (chia)* seeds extract as a reductant and stabilizer to prepare nickel oxide nanoparticles. In another study, Al-Qasmi et al. [51] reported successfully synthesizing copper oxide nanoparticles by using chia seed extract. The authors reported chia seeds as a suitable stabilizing substance for the green synthesis of nanoparticles, which showed comparable efficiency to conventional reduction procedures using hazardous polymers or surfactants.

Chitosan coated SPIONs (Fe_3O_4@CS core–shell)

To cover the MNPs with chitosan, 10.0 mg of low molecular weight chitosan was dissolved in 0.05% acetic acid solution (50 mL). In the following, the chitosan solution was added to the synthesized magnetic nanoparticles (0.1 g), which were then collected by an external magnet and washed with deionized water. After being separated, the precipitate that contained chitosan-coated magnetic nanoparticles was freeze-dried at − 80 °C for 24 h.

Loading of OXA and IRI on chitosan-coated SPIONs (Fe_3O_4–OXA@CS core–shell and Fe_3O_4–IRI@CS core–shell)

The Fe_3O_4@CS core–shell (10.0 mg) was dispersed with oxaliplatin (5.0 mL, 1.0 mg/mL) to have the obtained solution stirred for 48 h. After being centrifuged, the precipitate was lyophilized for 2 d, while in similar conditions, irinotecan (20 mg/mL) was loaded onto the surface of nanoparticles as well.

MTT assay

MTT assay was used to investigate the cell viability and toxicity effect of nano drugs on CT-26 cells. For this purpose, 2×10^4 CT-26 cells in each well of 96-well plate were treated with Fe_3O_4–OXA@CS core–shell and Fe_3O_4–IRI@CS core–shell (0, 8, 16, 32, 62.5, 125, 250, and 500 pm) to be incubated for 24 h. Moreover, 10 µL of 5% MTT solution was added to determine the cell viability, which was incubated in dark for 4 h. The produced formazan crystals were dissolved in DMSO to have the cell viability measured by a plate-reader at $\lambda_{max} = 570$ nm. Finally, the percentage of live cells in each concentration of treatment was calculated through the application of Prism Graphpad software using the following equation:

$$\text{Cell viability}(\%) = [\text{Adsrop}]\text{s}/\text{Ardorp}] \times 100$$

[Adsorp]s and [Adsorp] stand for the absorbance of treated samples and the control, respectively.

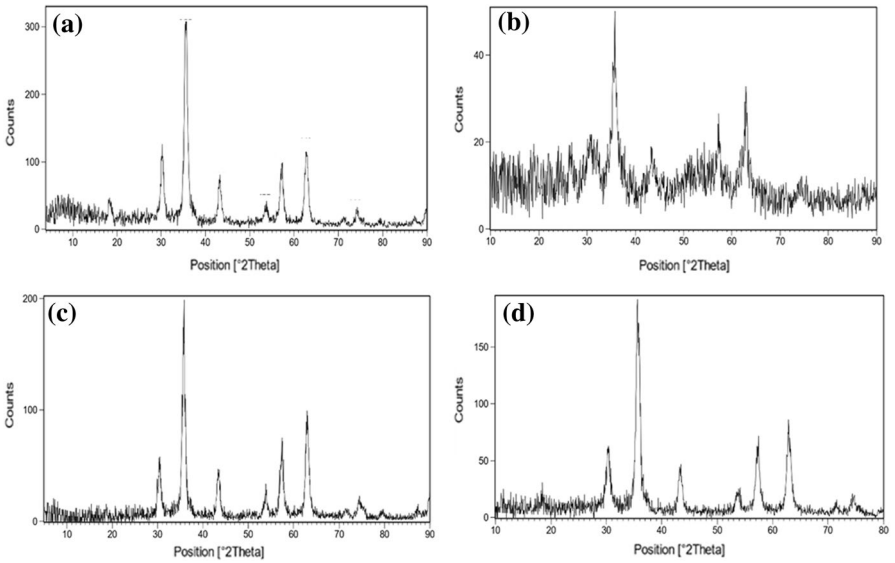

Fig. 2 The XRD patterns of the Fe_3O_4 SPIONs, Fe_3O_4@CS core–shell, Fe_3O_4–OXA@CS core–shell, and Fe_3O_4–IRI@CS core–shell

Result and discussion

XRD pattern

The obtained XRD analyses exhibited the successful synthesis of Fe_3O_4 nanoparticles (Fig. 2) [53]. The structure is compatible with Iron oxide and the reference code of 01-075-1609 (JCPDS code:031156) [54], which was crystallized in an orthorhombic crystal system (Space group: Imma, space group number: 74) [55]. The related calculated hkl (2θ, intensity) values were reported to be 011 (18.28°, 12.8%), 112 (30.12°, 33.1%), 200 (30.21°, 23.7%), 121 (35.43°, 82.2%), 103 (35.54°, 100%), 004 (43.12°, 27.3%), 132 (53.39°, 5.5%), 204 (53.6°, 6%), 231 (56.97°, 20.9%), 321 (57.09°, 21.3%), 041 (62.43°, 9.6%), 224 (62.61°, 36.4%), 400 (62.82°, 22.4%), 116 (71.02°, 2.4%), 420 (71.19°, 1.6%), 143 (73.92°, 3.9%), 305 (74.17°, 3.7%), 413 (74.25°, 3.6%), 422 (75.22°, 2.1%), 316 (86.99°, 1.4%), and 127 (89.7°, 4.1%). The experimental data clearly have displayed 2θ (intensity) values of 18.28° (10.9%), 30.20° (34.56%), 35.43° (95.81%), 35.73° (100), 43.19° (22%), 53.68° (6.4%), 57.18° (25.8%), 62.79° (37.43%), 71.21° (3.5%), 74.28° (6.7%), and 87.16° (3.18%). According to the results, the crystallinity of Fe_3O_4 nanoparticles faced a decrease after being coated by CS, in which the crystallite size experienced the same fate as well. Also, outcomes indicated that the orthorhombic crystal system remained intact after the CS coating and OXA and IRI loading. the Debye Scherrer equation (Eq. 1) was used to calculate the crystallite sizes of SPIONs, Fe_3O_4@CS core–shell, Fe_3O_4–OXA@CS core–shell, and Fe_3O_4–IRI@CS core–shell, which were observed to be 36.9 nm, 11.1 nm, 29.53 nm, and 25.33 nm, respectively. As an

interesting phenomenon, the drug loading leads to an increase in crystallitty compared to the Fe_3O_4@CS core–shell.

$$D = \frac{k\lambda}{\beta \cos\theta} \tag{1}$$

where $k = 0.9$, D is crystal size, λ is 0.154 nm, θ is the diffraction angle, and β would be the FWHM, in terms of radians [56].

FTIR

The changes in functionalities of SPIONs, Fe_3O_4@CS core–shell, Fe_3O_4–OXA@CS core–shell, and Fe_3O_4–IRI@CS core–shell were displayed throughout their FTIR spectroscopy (Fig. 3). The major IR adsorption bands of Fe_3O_4 nanoparticles were observed at 562 cm^{-1} and 628 cm^{-1}, indicating the formation of spinel (AB_2O_4) structure, while the O–H stretching (υ_{OH}) and Bending (δH_2O) were detected at 1677 cm^{-1} and 3438 cm^{-1} [57, 58]. Considering the few layers of CS that enveloped around Fe_3O_4 nanoparticles, only one region of the spectrum with no interferences was usable for analyzing the presence of CS within Fe_3O_4@CS core–shell. Accordingly, the COH and C–O–C vibrations were perceived in the region of 1000–1450 cm^{-1} without any specific sharp IR adsorption bands, which could be related to the presence of CS. After the loading process, the O–H stretching (υ_{OH})

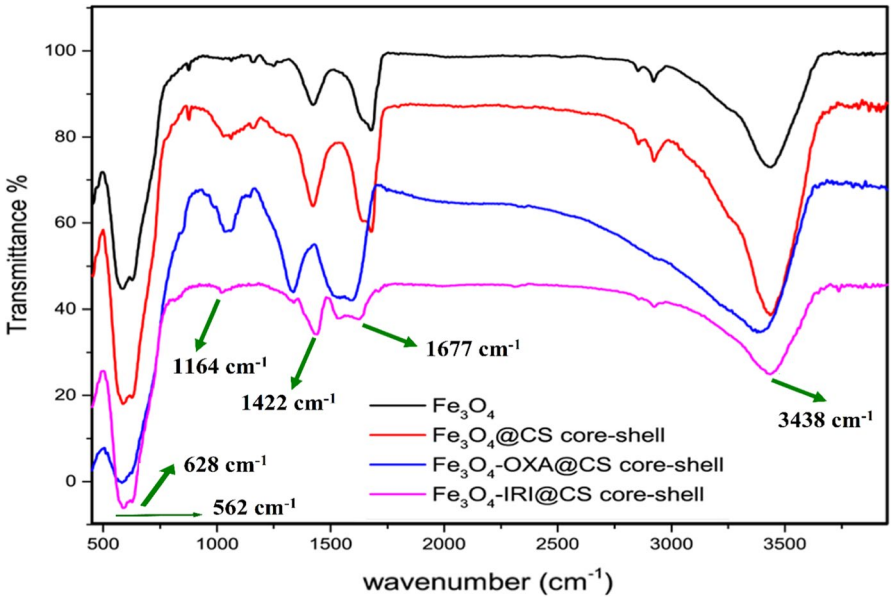

Fig. 3 The FTIR analyzes Fe_3O_4 nanoparticles, Fe_3O_4@CS core–shell, Fe_3O_4–OXA@CS core–shell, and Fe_3O_4–IRI@CS core–shell

was shifted towards lower wavelengths due to the formation of hydrogen bonds with OXA and IRI [59].

UV–Vis

To confirm the production of Fe_3O_4 nanoparticles by the usage of aqueous chia seed extract, the UV–Vis spectrum was recorded to provide data on the absorption spectrum of produced nanoparticles (Fig. 4). In this spectrum, the appeared peak at 290 nm indicated the production of Fe_3O_4 nanoparticles, which was associated with the ligand-to-metal charge transfer (LMCT) [60]. The optical properties of nanomaterial such as absorption and reflection differ from properties exhibited by the same bulk material. When the particle size becomes less than the wavelength of the incident radiation, the surface plasmon resonance phenomenon becomes dominant to control the optical properties of nanomaterials. The surface plasmon resonance is the result of coherent excitation of the free electrons of the nanomaterials, which are present in the conduction band and their in-phase resonance oscillations with the applied light energy. Thus nanomaterials can produce surface plasmon resonance, unlike bulk materials [61].

TEM images of Fe_3O_4@CS Core–shell

The TEM images of Fe_3O_4@CS core–shell at different magnifications, presented in Fig. 5, demonstrate their almost spherical and uniformed shape. However, unfortunately, there are signs of agglomeration as well, while the TEM images of chitosan-coated nanoparticles did not display the core–shell structure. The obtained

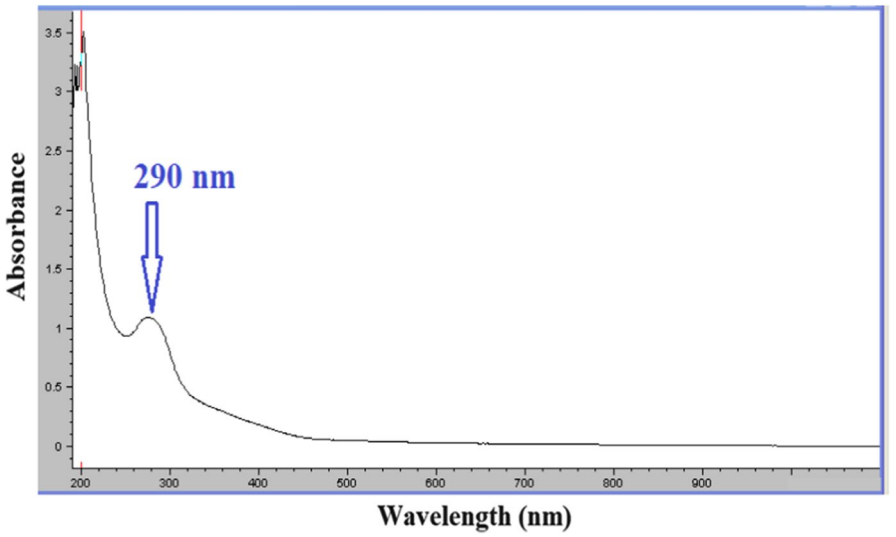

Fig. 4 UV–Vis spectrum of Fe_3O_4 nanoparticles

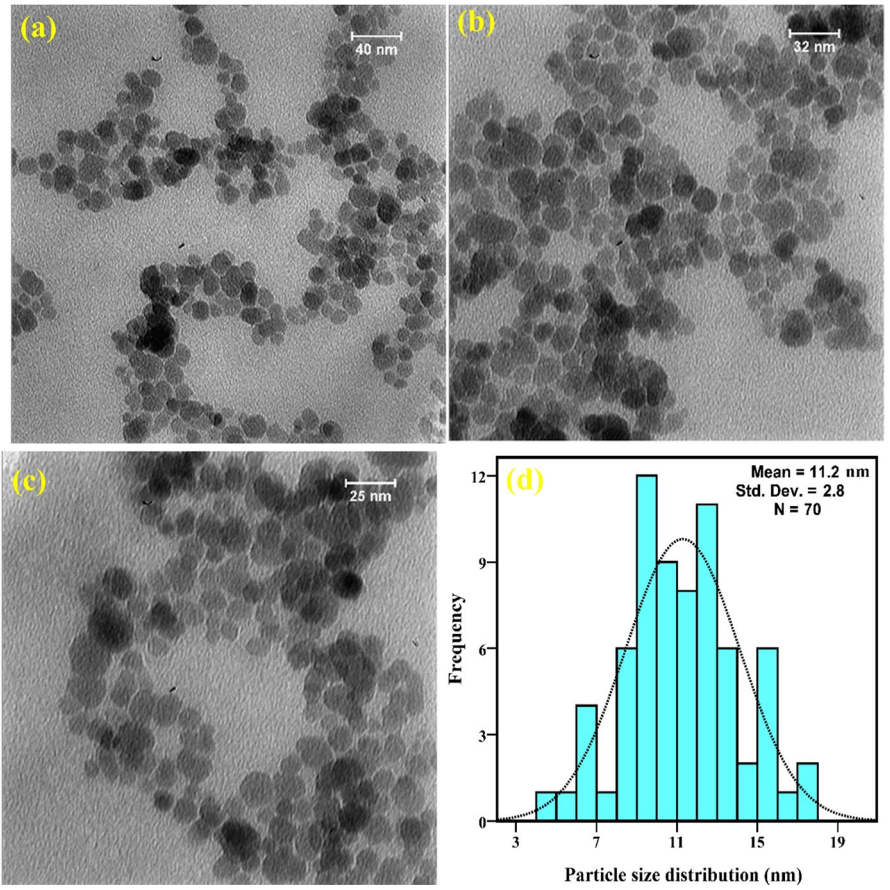

Fig. 5 The TEM images in scales 40 nm (**a**), 32 nm (**b**), and 25 nm (**c**), and particle size distribution (**d**) of Fe_3O_4@CS core–shell

particle size distribution from the performed analysis displayed a mean diameter of 36.77 nm. The particle agglomeration caused an increase in the size range, nearly up to 300 nm, leading to a large standard deviation relative to the mean diameter [62].

FESEM

The morphologies of Fe_3O_4 nanoparticles, Fe_3O_4@CS core–shell, Fe_3O_4–OXA@CS core–shell, and Fe_3O_4–IRI@CS core–shell were investigated through the application of FESEM images (Fig. 6). In conformity to results, the nanoscopic particles in each sample contained a spherical morphology. The observed morphological changes after CS coating and IRI loading were not apparent and changes in agglomeration, shape, and size were negligible, however, there was more agglomeration in the case of Fe_3O_4–OXA@CS core–shell than the other samples. It appears that the final morphology of the Fe_3O_4–OXA@CS core–shell was also spherical and remained intact.

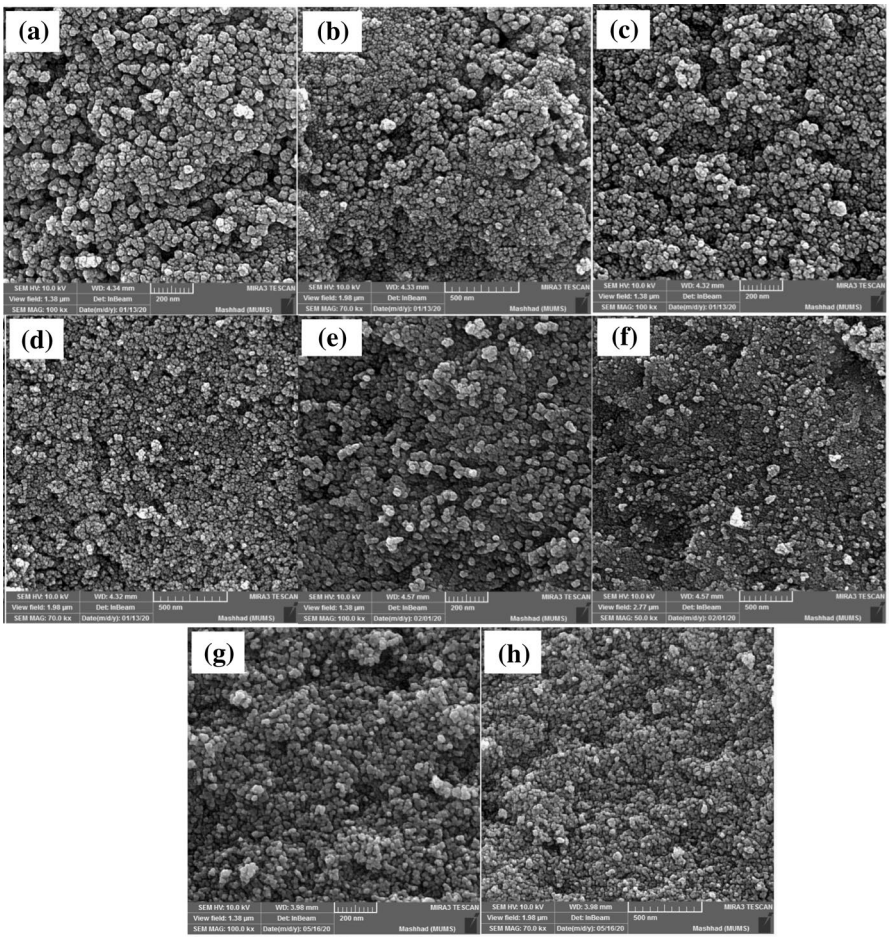

Fig. 6 The FESEM images of Fe_3O_4 nanoparticles (**a**, **b**), Fe_3O_4@CS core–shell (**c**, **d**), Fe_3O_4–OXA@CS core–shell (**e**, **f**), and Fe_3O_4–IRI@CS core–shell (**g**, **h**)

The energy dispersive X-ray analysis (EDX) was used in this study to investigate the qualitative elemental composition of the samples. EDX analysis of Fe_3O_4 nanoparticles, Fe_3O_4@CS core–shell, Fe_3O_4–OXA@CS core–shell, and Fe_3O_4–IRI@CS core–shell exhibited the compositional changes of the samples (Fig. 7). The Fe_3O_4 nanoparticles, which were composed of oxygen and iron while being coated with CS, were observed to hold the presence of nitrogen and carbon as well. Next to being loaded with OXA, the presence of platinum was confirmed by PtM_α, PtM_β, and PtL_α. On the other hand similar to CS, IRI is an organic compound that contains carbon, nitrogen, and oxygen, which consequently resulted in the lack of qualitative elemental changes. The obtained results were indicative of the high purity of synthesized nanoparticles.

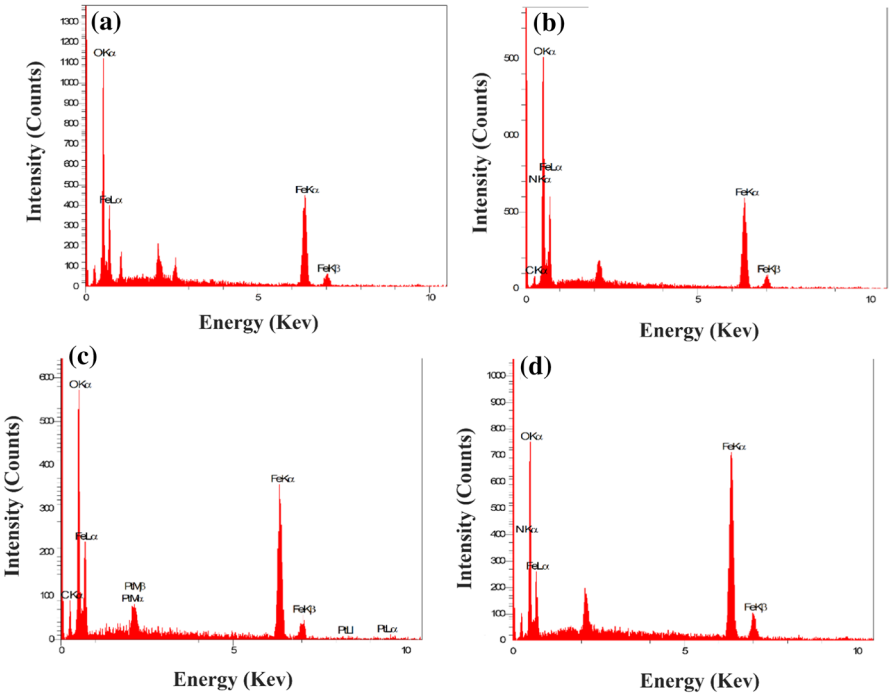

Fig. 7 The EDX of Fe_3O_4 nanoparticles (**a**), Fe_3O_4@CS core–shell (**b**), Fe_3O_4–OXA@CS core–shell (**c**), and Fe_3O_4–IRI@CS core–shell (**d**)

DLS

The induced changes in the hydrodynamic diameter of Fe_3O_4 nanoparticles, Fe_3O_4@CS core–shell, Fe_3O_4–OXA@CS core–shell, and Fe_3O_4–IRI@CS core–shell were evaluated by the means of DLS analysis (Fig. 8). The achieved Z-averages (polydispersity index, PDI) from DLS analysis (Fig. 8) displayed that the uncoated Fe_3O_4 nanoparticles have a size of about 38.42 (0.15) nm. Additionally, after coating chitosan, the size of Fe_3O_4@CS core–shell has changed to 74.21 (0.22) nm which approves the presence of a new layer on nanoparticles. Also, the drug loading caused the size of Fe_3O_4–OXA@CS core–shell, and Fe_3O_4–IRI@CS core–shell to be 92.5 (0.24), and 172.55 (0.26) nm. Although TEM and crystallite sizes of Fe_3O_4 nanoparticles were indicative of low clustering/ agglomeration, on the other hand, the hydrodynamic size of Fe_3O_4@CS core–shell was nearly 7-times larger than its crystallite size. The core–shell formation and presence of different hydroxyl and amine groups in the composition of CS caused a noticeable increase in the hydrodynamic sizes. The hydrodynamic size of Fe_3O_4@CS core–shell was affected by the formation of Hydrogen bonds with water, which greatly increased their sizes. The clustering of more than two particles in the aqueous media can stand as another possible explanation for this observation. After the loading of OXA and IRI, the sizes were increased even more than in the case of Fe_3O_4@CS core–shell, which resulted in enlarging

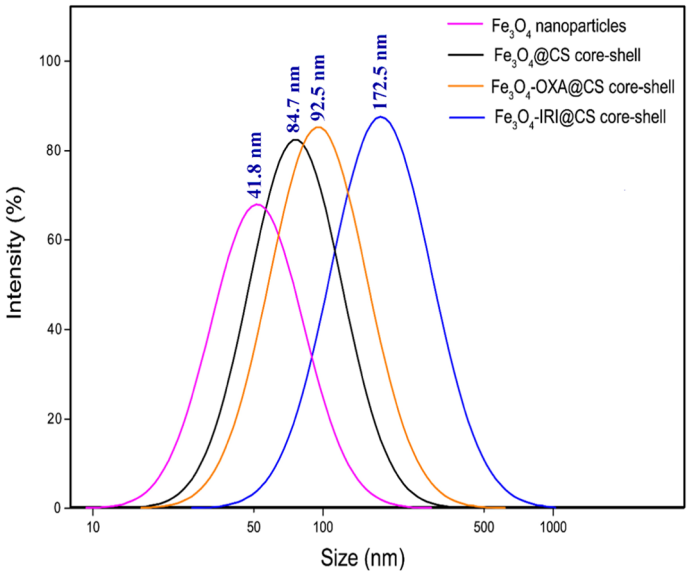

Fig. 8 DLS analyses values of Fe_3O_4 nanoparticles, Fe_3O_4@CS core–shell, Fe_3O_4–OXA@CS core–shell, and Fe_3O_4–IRI@CS core–shell

the hydrodynamic sizes. The FESEM image of Fe_3O_4–OXA@CS core–shell demonstrated the formation of aggregated nanoparticles and due to the tendency of DLS to display larger particles, larger hydrodynamic sizes were perceivable throughout the results. The zeta potentials were measured at pH = 6.8 while negative outcomes were reported for all the samples of the aqueous medium, which can be regarded as a sign of stability in water. The obtained zeta potentials of Fe_3O_4 nanoparticles, Fe_3O_4@CS core–shell, Fe_3O_4–OXA@CS core–shell, and Fe_3O_4–IRI@CS core–shell were − 16.99, − 12.99, − 16.72, and − 14.28 mV, respectively. Result of Zeta potential was presented in Table 1.

VSM

The saturation magnetization (Ms) of samples was determined by the application of VSM at room temperature (Fig. 9). The suitable conditions for achieving a superparamagnetic behavior were associated with the size of nanoparticles, which

Table 1 Result of Zeta potential

Sample	Zeta Potential (mV)
Fe_3O_4	− 16.99
Fe_3O_4@CS core–shell	− 12.99
Fe_3O_4–OXA@CS core–shell	− 16.72
Fe_3O_4–IRI@CS core–shell	− 14.28

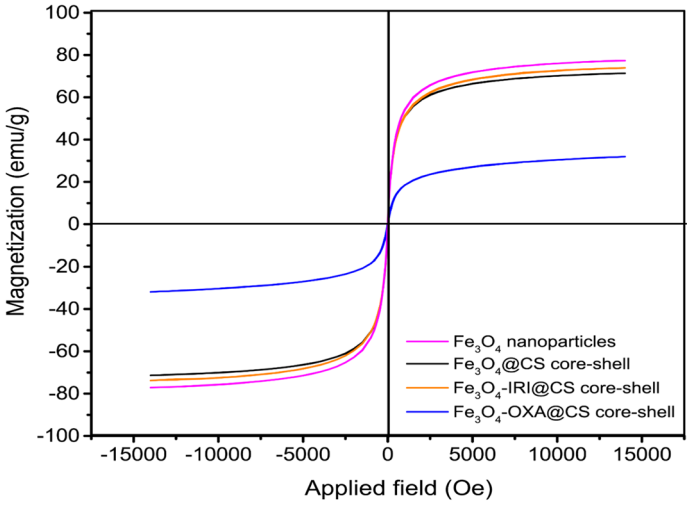

Fig. 9 The magnetization of the Fe_3O_4 nanoparticles, Fe_3O_4@CS core–shell, Fe_3O_4–OXA@CS core–shell, and Fe_3O_4–IRI@CS core–shell

was required to be between 3–50 nm and be lower than the superparamagnetic critical size [63]. The Ms values of Fe_3O_4 nanoparticles, Fe_3O_4@CS core–shell, Fe_3O_4–OXA@CS core–shell, and Fe_3O_4–IRI@CS core–shell were 77.4, 71.43, 31.91, and 73.91 emus.g^{-1}, respectively. There were no remanence magnetization and coercivity observed throughout the samples. The Ms values of Fe_3O_4@CS core–shell and Fe_3O_4–IRI@CS core–shell were slightly reduced after the formation of CS core–shell and IRI loading, which could be mainly attributed to the diamagnetic nature of CS and IRI. However, in the case of Fe_3O_4–OXA@CS core–shell, the value of Ms was drastically declined as a result of CS core–shell, OXA loading, and the higher agglomeration of nanoparticles. Their presence causes synergistic effects by disrupting the surface moments, reducing MS, and causing negative influences on magnetism [64].

MTT assay

The anticancer attributes of Fe_3O_4@CS core–shell, Fe_3O_4–OXA@CS core–shell, and Fe_3O_4–IRI@CS core–shell against CT26 cancer cells were investigated by experimenting samples with different concentrations and doses of 0, 4, 8, 16, 31, 62, 125, 250, 500 ppm (Fig. 10). The obtained results indicated that in comparison to Fe_3O_4@CS core–shell, which demonstrated lower cytotoxicity against colorectal cancer cells (IC_{50} = 246.6 ppm), the cases of IC_{50s} of Fe_3O_4–OXA@CS core–shell (IC_{50} = 79.6 ppm) and Fe_3O_4–IRI@CS core–shell (IC_{50} = 61.1 ppm) were decreased more than 3- and 4-times, respectively. Considering the apparent effect of drug loading on the potency of nano drugs, the applicability of magnetic nanoparticles in designing drug delivery systems can be suggested [20].

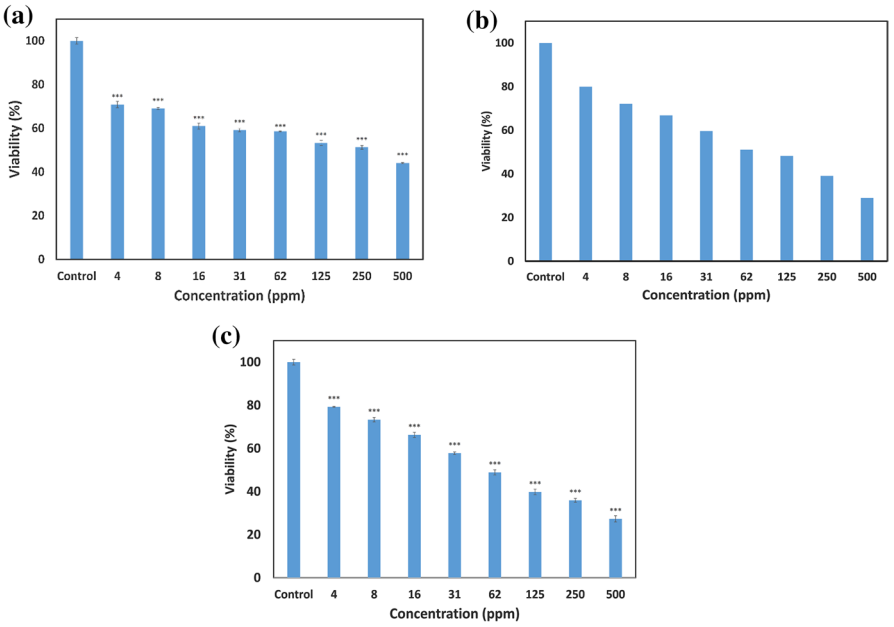

Fig. 10 The MTT of Fe_3O_4@CS core–shell, Fe_3O_4–OXA@CS core–shell, and Fe_3O_4–IRI@CS core–shell against CT 26 cancer cells

Discussion

To investigate drug delivery systems using Fe_3O_4@CS core–shell, the Fe_3O_4@CS core–shell and guest interactions are needed to be optimized to control spontaneous drug release [65–69]. Fe_3O_4@CS core–shell appears to be effective for this aim. The use of nanomaterials such as magnetic nanoparticles can be used to facilitate drug release by a stimulus [70]. For example, the superparamagnetic chitosan nanocomplexes were examined for colorectal tumor-targeted delivery of irinotecan [71]. In another study of TiO_2 and iron oxide nanoparticles was used for cancer therapy: surface chemistry and biological implications [72]. The other nanomaterials were magnetic functionalized nanoparticles for the responsive and targeted drug delivery on colorectal cancer therapy [73]. Also, magnetic nanoparticles were used in cancer therapy and diagnosis [74]. Nanomaterials, including magnetic nanoparticles, appear to be effective in inducing drug release by a stimulus. The magnetic nanoparticles can be used applied to design drug delivery systems based on Fe_3O_4@CS core–shell, which could lead to a better release. Herein, the Fe_3O_4@CS core–shell was used for the first time to examine the character of the Fe_3O_4–OXA@CS core–shell and Fe_3O_4–IRI@CS core–shell against CT-26 cancer cells. The XRD analyses have displayed the successful synthesis of the Fe_3O_4 nanoparticles and Fe_3O_4@CS core–shell. Also, FTIR analyses have been approved the presence of C-H stretching of the OXA after drug loading. The XRD pattern approved that the structure was remained whole after drug loading. The crystallity structures and FESEM images evidente aggregation is much more in the aqueous media. Despite

all these barriers, the powders thoroughly were suspended in the solution for biological experiments. The cytotoxicities of drug-loaded nanoparticles were exceedingly increased when being compared to the case of Fe_3O_4@CS core–shell.

Conclusions and future prospects

In this study, the green synthesis of the magnetic nanoparticle by the usage of chia seed extracts was introduced to display the capability of these particles for being applied in drug delivery approaches. The flexibility of magnetic nanoparticles for tailoring better nanocarriers by the usage of biopolymers, such as chitosan, has caught the attention of many since this method can result in increasing the biocompatibility and drug loading capacity of surfaces. According to the performed analyses, chia seed water extract can form uniformed spherical nanoparticles with the ability to display superparamagnetism behaviors. The cytotoxicity of drug-loaded nanoparticles executed a better eradication of CT-26 colorectal cancer cells when being compared to the outcomes of Fe_3O_4@CS core–shell. The facile and green synthesizing methods proved to be useful in the synthesis of new and effective drug delivery systems. A thorough study of the characteristics of the formed targeted delivery systems including biocompatibility, biodegradation, toxicity, and low cellular stability and dissemination of targeting based on demand in the human body is essential. Continuous work is needed to discover the mechanism by which the prepared magnetic nanoparticles enter human diseased cells and how they interact via human cancer cells, as well as the mechanism of cell death/body metabolism pathways. We firmly believe that these obstacles will be overcome through our relentless efforts. However, there is no doubt that Fe_3O_4 NP-based targeted drug /gene delivery systems are new and very valuable methods that play a pivotal role in biomedicine and open up new fields of research.

Acknowledgments The technical support for this work was provided by Islamic Azad University of Quchan and Mashhad University of Medical Sciences based on the MS thesis of Ms. N. Farmanbar.

Funding None.

Declarations

Conflict of interest The authors declare that they have no conflict of interest.

Ethical approval For this type of study, the ethical approval was not.

References

1. Hashemzadeh A, Drummen G, Avan A, Darroudi M, Khazaei M, Khajavian R, Rangrazi A, Mirzaei M (2021) When a metal-organic framework mediated smart drug delivery meets gastrointestinal cancers. J Mater Chem B
2. Asgharzadeh F, Hashemzadeh A, Yaghoubi A, Avan A, Nazari SE, Soleimanpour S, Hassanian SM, Ferns GA, Rahmani F, Khazaei M (2021) Therapeutic effects of silver nanoparticle containing sulfasalazine on DSS-induced colitis model. J Drug Deliv Sci Technol 61:102133

3. Fereydouni N, Movaffagh J, Amiri N, Darroudi S, Gholoobi A, Goodarzi A, Hashemzadeh A, Darroudi M (2021) Synthesis of nano-fibers containing nano-curcumin in zein corn protein and its physicochemical and biological characteristics. Sci Rep 11(1):1–15
4. Naeem M, Awan UA, Subhan F, Cao J, Hlaing SP, Lee J, Im E, Jung Y, Yoo J-W (2020) Advances in colon-targeted nano-drug delivery systems: challenges and solutions. Arch Pharmacal Res 43(1):153–169
5. Marques A, Costa P, Velho S, Amaral M (2020) Functionalizing nanoparticles with cancer-targeting antibodies: a comparison of strategies. J Control Release 320:180–200
6. Moballegh Nasery M, Abadi B, Poormoghadam D, Zarrabi A, Keyhanvar P, Khanbabaei H, Ashrafizadeh M, Mohammadinejad R, Tavakol S, Sethi G (2020) Curcumin delivery mediated by bio-based nanoparticles: a review. Molecules 25(3):689
7. Gong F, Yang N, Wang X, Zhao Q, Chen Q, Liu Z, Cheng L (2020) Tumor microenvironment-responsive intelligent nanoplatforms for cancer theranostics. Nano Today 32:100851
8. Kievit FM, Zhang M (2011) Surface engineering of iron oxide nanoparticles for targeted cancer therapy. Acc Chem Res 44(10):853–862
9. Dadfar SM, Roemhild K, Drude NI, von Stillfried S, Knüchel R, Kiessling F, Lammers T (2019) Iron oxide nanoparticles: diagnostic, therapeutic and theranostic applications. Adv Drug Deliv Rev 138:302–325
10. Ulbrich K, Hola K, Subr V, Bakandritsos A, Tucek J, Zboril R (2016) Targeted drug delivery with polymers and magnetic nanoparticles: covalent and noncovalent approaches, release control, and clinical studies. Chem Rev 116(9):5338–5431
11. Wahajuddin SA (2012) Superparamagnetic iron oxide nanoparticles: magnetic nanoplatforms as drug carriers. Int J Nanomed 7:3445
12. Dulińska-Litewka J, Łazarczyk A, Hałubiec P, Szafrański O, Karnas K, Karewicz A (2019) Superparamagnetic iron oxide nanoparticles—current and prospective medical applications. Materials 12(4):617
13. Mohammed L, Gomaa HG, Ragab D, Zhu J (2017) Magnetic nanoparticles for environmental and biomedical applications: a review. Particuology 30:1–14
14. Khan A, Sahu NK (2020) Folate encapsulation in PEG-diamine grafted mesoporous Fe3O4 nanoparticles for hyperthermia and in vitro assessment. IET Nanobiotechnol 14(9):881–888
15. Sullivan MV, Stockburn WJ, Hawes PC, Mercer T, Reddy SM (2020) Green synthesis as a simple and rapid route to protein modified magnetic nanoparticles for use in the development of a fluorometric molecularly imprinted polymer-based assay for detection of myoglobin. Nanotechnology 32(9):095502
16. Rahmani R, Gharanfoli M, Gholamin M, Darroudi M, Chamani J, Sadri K, Hashemzadeh A (2020) Plant-mediated synthesis of superparamagnetic iron oxide nanoparticles (SPIONs) using aloe vera and flaxseed extracts and evaluation of their cellular toxicities. Ceram Int 46(3):3051–3058
17. Park SB, Goldstein D, Krishnan AV, Lin CSY, Friedlander ML, Cassidy J, Koltzenburg M, Kiernan MC (2013) Chemotherapy-induced peripheral neurotoxicity: a critical analysis. CA Cancer J Clin 63(6):419–437
18. Argyriou AA, Bruna J, Marmiroli P, Cavaletti G (2012) Chemotherapy-induced peripheral neurotoxicity (CIPN): an update. Crit Rev Oncol Hematol 82(1):51–77
19. Oun R, Moussa YE, Wheate NJ (2018) The side effects of platinum-based chemotherapy drugs: a review for chemists. Dalton Trans 47(19):6645–6653
20. Tabasi H, Hamed Mosavian MT, Sabouri Z, Khazaei M, Darroudi M (2021) pH-responsive and CD44-targeting by Fe3O4/MSNs-NH2 nanocarriers for Oxaliplatin loading and colon cancer treatment. Inorg Chem Commun 125:108430. https://doi.org/10.1016/j.inoche.2020.108430
21. Johnstone TC, Suntharalingam K, Lippard SJ (2016) The next generation of platinum drugs: targeted Pt (II) agents, nanoparticle delivery, and Pt (IV) prodrugs. Chem Rev 116(5):3436–3486
22. Gholoobi A, Meshkat Z, Abnous K, Ghayour-Mobarhan M, Ramezani M, Homaei Shandiz F, Verma KD, Darroudi M (2017) Biopolymer-mediated synthesis of Fe3O4 nanoparticles and investigation of their in vitro cytotoxicity effects. J Mol Struct 1141:594–599. https://doi.org/10.1016/j.molstruc.2017.04.024
23. Yew YP, Shameli K, Miyake M, Khairudin NBBA, Mohamad SEB, Naiki T, Lee KX (2020) Green biosynthesis of superparamagnetic magnetite Fe3O4 nanoparticles and biomedical applications in targeted anticancer drug delivery system: a review. Arab J Chem 13(1):2287–2308
24. Aisida SO, Alnasir MH, Botha S, Bashir A, Bucher R, Ahmad I, Zhao T-k, Maaza M, Ezema FI (2020) The role of polyethylene glycol on the microstructural, magnetic and specific absorption

rate in thermoablation properties of Mn-Zn ferrite nanoparticles by sol–gel protocol. Eur Polym J 132:109739
25. Vangijzegem T, Stanicki D, Laurent S (2019) Magnetic iron oxide nanoparticles for drug delivery: applications and characteristics. Exp Opin Drug Deliv 16(1):69–78
26. Han H, Hou Y, Chen X, Zhang P, Kang M, Jin Q, Ji J, Gao M (2020) Metformin-induced stromal depletion to enhance the penetration of gemcitabine-loaded magnetic nanoparticles for pancreatic cancer targeted therapy. J Am Chem Soc 142(10):4944–4954
27. Zhang W, Taheri-Ledari R, Hajizadeh Z, Zolfaghari E, Ahghari MR, Maleki A, Hamblin MR, Tian Y (2020) Enhanced activity of vancomycin by encapsulation in hybrid magnetic nanoparticles conjugated to a cell-penetrating peptide. Nanoscale 12(6):3855–3870
28. Liu D, Hong Y, Li Y, Hu C, Yip T-C, Yu W-K, Zhu Y, Fong C-C, Wang W, Au S-K (2020) Targeted destruction of cancer stem cells using multifunctional magnetic nanoparticles that enable combined hyperthermia and chemotherapy. Theranostics 10(3):1181
29. Ebrahim SA, Ashtari A, Pedram MZ, Ebrahim NA (2019) Publication trends in drug delivery and magnetic nanoparticles. Nanoscale Res Lett 14(1):1–14
30. Ades S (2009) Adjuvant chemotherapy for colon cancer in the elderly: moving from evidence to practice. Oncology 23(2):162–162
31. Niu H, Meng Z, Cai Y (2012) Fast defluorination and removal of norfloxacin by alginate/Fe@ Fe3O4 core/shell structured nanoparticles. J Hazard Mater 227:195–203
32. Justin C, Samrot AV, Sahithya CS, Bhavya KS, Saipriya C (2018) Preparation, characterization and utilization of coreshell super paramagnetic iron oxide nanoparticles for curcumin delivery. PloS One 13(7):e0200440
33. Karimi M, Ghasemi A, Zangabad PS, Rahighi R, Basri SMM, Mirshekari H, Amiri M, Pishabad ZS, Aslani A, Bozorgomid M (2016) Smart micro/nanoparticles in stimulus-responsive drug/gene delivery systems. Chem Soc Rev 45(5):1457–1501
34. Dutta RK, Sahu S (2012) Development of oxaliplatin encapsulated in magnetic nanocarriers of pectin as a potential targeted drug delivery for cancer therapy. Res Pharma Sci 2:38–45
35. Munaweera I, Shi Y, Koneru B, Saez R, Aliev A, Di Pasqua AJ, Balkus KJ Jr (2015) Chemoradiotherapeutic magnetic nanoparticles for targeted treatment of nonsmall cell lung cancer. Mol Pharm 12(10):3588–3596
36. Fawcett D, Verduin JJ, Shah M, Sharma SB, Poinern GEJ (2017) A review of current research into the biogenic synthesis of metal and metal oxide nanoparticles via marine algae and seagrasses. J Nanosci 2017
37. Parsian M, Unsoy G, Mutlu P, Yalcin S, Tezcaner A, Gunduz U (2016) Loading of Gemcitabine on chitosan magnetic nanoparticles increases the anti-cancer efficacy of the drug. Eur J Pharmacol 784:121–128
38. Wu D, Zhu L, Li Y, Wang H, Xu S, Zhang X, Wu R, Yang G (2020) Superparamagnetic chitosan nanocomplexes for colorectal tumor-targeted delivery of irinotecan. Int J Pharm 584:119394
39. 39. Zhang Y, Qi J, Chen H, Xiong C (2021) Corrigendum to "Amphiphilic diblock copolymers inhibit the formation of encrustation on the surface of biodegradable ureteral stents in vitro and in vivo" [Colloids Surf. A: Physicochem. Eng. Asp. 610 (2021) 125667]. Colloids Surf A Physicochem Eng Asp 625:126997. https://doi.org/10.1016/j.colsurfa.2021.126997
40. Hayashi K, Ono K, Suzuki H, Sawada M, Moriya M, Sakamoto W, Yogo T (2010) High-frequency, magnetic-field-responsive drug release from magnetic nanoparticle/organic hybrid based on hyperthermic effect. ACS Appl Mater Interfaces 2(7):1903–1911
41. Saboktakin MR, Tabatabaie R, Maharramov A, Ramazanov MA (2010) Synthesis and characterization of superparamagnetic chitosan–dextran sulfate hydrogels as nano carriers for colon-specific drug delivery. Carbohyd Polym 81(2):372–376
42. Denadai ÂM, Ianzer D, Alcântara AFdC, Santoro MM, Santos CF, Lula IS, de Camargo AC, Faljoni-Alario A, dos Santos RA, Sinisterra RD (2007) Novel pharmaceutical composition of bradykinin potentiating penta peptide with β-cyclodextrin: physical–chemical characterization and antihypertensive evaluation. Int J Pharm 336(1):90–98
43. Zambito Y, Pedreschi E, Di Colo G (2012) Is dialysis a reliable method for studying drug release from nanoparticulate systems?—a case study. Int J Pharm 434(1–2):28–34
44. Subbiah R, Ramalingam P, Ramasundaram S, Park K, Ramasamy MK, Choi KJ (2012) N, N, N-Trimethyl chitosan nanoparticles for controlled intranasal delivery of HBV surface antigen. Carbohyd Polym 89(4):1289–1297

45. Brito E, Gomes D, Cid CP, de Araújo J, Bohn F, Streck L, Fonseca J (2019) Superparamagnetic magnetite/IPEC particles. Colloids Surf A 560:376–383
46. Ag M, AM ES, MS S, (2013) Current situation of water pollution and its effect on aquatic life in Egypt. Egy J Occup Med 37(1):95–115
47. de Campo C, Dos Santos PP, Costa TMH, Paese K, Guterres SS, de Oliveira RA, Flôres SH (2017) Nanoencapsulation of chia seed oil with chia mucilage (Salvia hispanica L.) as wall material: Characterization and stability evaluation. Food Chem 234:1–9
48. Kuznetcova DV, Linder M, Jeandel C, Paris C, Desor F, Baranenko DA, Nadtochii LA, Arab-Tehrany E, Yen FT (2020) Nanoliposomes and nanoemulsions based on chia seed lipids: preparation and characterization. Int J Mol Sci 21(23):9079
49. da Silva SF, de Campo C, Paese K, Guterres SS, Costa TMH, Flôres SH (2019) Nanoencapsulation of linseed oil with chia mucilage as structuring material: characterization, stability and enrichment of orange juice. Food Res Int 120:872–879
50. Hernández-Morales L, Espinoza-Gómez H, Flores-López LZ, Sotelo-Barrera EL, Núñez-Rivera A, Cadena-Nava RD, Alonso-Núñez G, Espinoza KA (2019) Study of the green synthesis of silver nanoparticles using a natural extract of dark or white Salvia hispanica L. seeds and their antibacterial application. Appl Surf Sci 489:952–961
51. Al-Qasmi N (2021) Facial eco-friendly synthesis of copper oxide nanoparticles using chia seeds extract and evaluation of its electrochemical activity. Processes 9(11):2027
52. Sabouri Z, Rangrazi A, Amiri MS, Khatami M, Darroudi M (2021) Green synthesis of nickel oxide nanoparticles using Salvia hispanica L. (chia) seeds extract and studies of their photocatalytic activity and cytotoxicity effects. Bioprocess Biosyst Eng 44(11):2407–2415. https://doi.org/10.1007/s00449-021-02613-8
53. Silva VAJ, Andrade PL, Silva MPC, Bustamante DA, De Los Santos Valladares L, Albino Aguiar J (2013) Synthesis and characterization of Fe3O4 nanoparticles coated with fucan polysaccharides. J Magn Magn Mater 343:138–143. https://doi.org/10.1016/j.jmmm.2013.04.062
54. Matei E, Predescu C, Berbecaru A, Predescu A, Trusca R (2011) Leaching tests for synthesized magnetite nanoparticles used as adsorbent for metal ions from liquid solutions. Dig J Nanomater Biostruct 6(4):1701–1708
55. Řezníček R, Chlan V, Štěpánková H, Novák P, Maryško M (2012) Magnetocrystalline anisotropy of magnetite. J Phys Condensed Matter 24(5):055501
56. Sahu D, Panda N, Acharya B, Panda A (2014) Enhanced UV absorbance and photoluminescence properties of ultrasound assisted synthesized gold doped ZnO nanorods. Opt Mater 36(8):1402–1407
57. Nalbandian L, Patrikiadou E, Zaspalis V, Patrikidou A, Hatzidaki E, Papandreou NC (2016) Magnetic Nanoparticles in medical diagnostic applications: synthesis, characterization and proteins conjugation. Curr Nanosci 12(4):455–468
58. Sahoo Y, Goodarzi A, Swihart MT, Ohulchanskyy TY, Kaur N, Furlani EP, Prasad PN (2005) Aqueous ferrofluid of magnetite nanoparticles: fluorescence labeling and magnetophoretic control. J Phys Chem B 109(9):3879–3885
59. Machodi MJ, Daramola MO (2019) Synthesis and performance evaluation of PES/chitosan membranes coated with polyamide for acid mine drainage treatment. Sci Rep 9(1):1–14
60. Balamurugan M, Saravanan S, Soga T (2014) Synthesis of iron oxide nanoparticles by using Eucalyptus globulus plant extract. e-J Surf Sci Nanotechnol 12:363–367
61. Adewuyi A, Lau WJ (2021) Chapter 3—nanomaterial development and its applications for emerging pollutant removal in water. In: Lau WJ, Faungnawakij K, Piyachomkwan K, Ruktanonchai UR (eds) Handbook of nanotechnology applications. Elsevier, pp 67–97. https://doi.org/10.1016/B978-0-12-821506-7.00003-X
62. Elahi B, Mirzaee M, Darroudi M, Kazemi Oskuee R, Sadri K, Amiri MS (2019) Preparation of cerium oxide nanoparticles in salvia macrosiphon boiss seeds extract and investigation of their photo-catalytic activities. Ceram Int 45(4):4790–4797. https://doi.org/10.1016/j.ceramint.2018.11.173
63. Jaiswal MK, Gogoi M, Dev Sarma H, Banerjee R, Bahadur D (2014) Biocompatibility, biodistribution and efficacy of magnetic nanohydrogels in inhibiting growth of tumors in experimental mice models. Biomater Sci 2(3):370–380. https://doi.org/10.1039/C3BM60225G
64. Dorniani D, Hussein MZB, Kura AU, Fakurazi S, Shaari AH, Ahmad Z (2012) Preparation of Fe3O4 magnetic nanoparticles coated with gallic acid for drug delivery. Int J Nanomed 7:5745

65. Huxford RC, Della Rocca J, Lin W (2010) Metal–organic frameworks as potential drug carriers. Curr Opin Chem Biol 14(2):262–268
66. Horcajada P, Gref R, Baati T, Allan PK, Maurin G, Couvreur P, Ferey G, Morris RE, Serre C (2012) Metal–organic frameworks in biomedicine. Chem Rev 112(2):1232–1268
67. Horcajada P, Chalati T, Serre C, Gillet B, Sebrie C, Baati T, Eubank JF, Heurtaux D, Clayette P, Kreuz C (2010) Porous metal–organic-framework nanoscale carriers as a potential platform for drug delivery and imaging. Nat Mater 9(2):172–178
68. Cunha D, Ben Yahia M, Hall S, Miller SR, Chevreau H, Elkaïm E, Maurin G, Horcajada P, Serre C (2013) Rationale of drug encapsulation and release from biocompatible porous metal–organic frameworks. Chem Mater 25(14):2767–2776
69. Hashemzadeh A, Drummen GP, Avan A, Darroudi M, Khazaei M, Khajavian R, Mirzaei Shahrabi M, Rangrazi A (2021) When a metal-organic framework mediated smart drug delivery meets gastrointestinal cancers. J Mater Chem B 50
70. Abney CW, Taylor-Pashow KM, Russell SR, Chen Y, Samantaray R, Lockard JV, Lin W (2014) Topotactic transformations of metal–organic frameworks to highly porous and stable inorganic sorbents for efficient radionuclide sequestration. Chem Mater 26(18):5231–5243
71. Wu D, Zhu L, Li Y, Wang H, Xu S, Zhang X, Wu R, Yang G (2020) Superparamagnetic chitosan nanocomplexes for colorectal tumor-targeted delivery of irinotecan. Int J Pharm 584:119394. https://doi.org/10.1016/j.ijpharm.2020.119394
72. Kawassaki RK, Romano M, Dietrich N, Araki K (2021) Titanium and iron oxide nanoparticles for cancer therapy: surface chemistry and biological implications. Front Nanotechnol 3(68). https://doi.org/10.3389/fnano.2021.735434
73. Darroudi M, Gholami M, Rezayi M, Khazaei M (2021) An overview and bibliometric analysis on the colorectal cancer therapy by magnetic functionalized nanoparticles for the responsive and targeted drug delivery. J Nanobiotechnol 19(1):399. https://doi.org/10.1186/s12951-021-01150-6
74. Farzin A, Etesami SA, Quint J, Memic A, Tamayol A (2020) Magnetic nanoparticles in cancer therapy and diagnosis. Adv Healthc Mater 9(9):1901058

Authors and Affiliations

Nadia Farmanbar[1] · Sharareh Mohseni[1] · Majid Darroudi[2,3]

[1] Department of Chemistry, Quchan Branch, Islamic Azad University, Quchan, Iran

[2] Nuclear Medicine Research Center, Mashhad University of Medical Sciences, Mashhad, Iran

[3] Department of Medical Biotechnology and Nanotechnology, Faculty of Medicine, Mashhad University of Medical Sciences, Mashhad, Iran